High Spatial Resolution Optical Fiber Two Color Pyrometer With Fast Response

A. Núñez Cascajero, A. Tapetado, and C. Vázquez, *Senior Member, IEEE*

***Abstract*—Among the different temperature measurement techniques providing micrometer resolution none of them provide fast response and easy access to close distances to the target surface in difficult to access areas. Optical fiber pyrometers provide that access but previous works used large optical fibers with numerical apertures limiting the minimum spot size to be measured. In this study, we propose a novel two colour optical fiber pyrometer based on a low diameter and numerical aperture optical fiber, low-noise photodetectors and high-gain transimpedance amplifiers with a high spatial resolution in the micrometre range and fast response. Using standard optical fibers and related devices provides also a low-cost system. The developed pyrometer presents a high spatial resolution of 16 μm for a target surface at 25 μm with a wide temperature range of 300 to 1200°C it being the highest spatial resolution for this kind of temperature systems. Theoretical analysis and measurements for different pyrometer configurations are reported. This study will help further the microthermography applications in machining processes.**

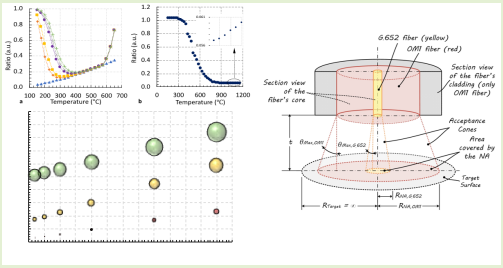

***Index Terms*— Multimode fiber, optical fiber, single mode fiber, spatial resolution, temperature measurement, two color pyrometer.**

I. Introduction

TEMPERATURE measurements can be done by contact (i.e. thermocouples) or non-contact (i.e. infrared (IR) cameras, pyrometers, among others) methods. In this paper, we focus on those based on the optical analysis of the infrared rays emitted by a heated surface. These non-contact measurements are less invasive and non-destructive.

The spatial resolution of the far field optical-temperature measurements is limited to a maximum of $\sim \lambda/2$, where λ is the wavelength that is being analysed. Infrared cameras for temperature measurement collect the infrared rays from the heated body. IR cameras with a standard objective allow spatial resolutions around 1 mm and must be equipped with an additional close-up lens to increase its spatial resolution up to $5 - 10$ μm [1], [2], with the consequent increasing cost. Even more, it is difficult to know the emissivity of the material which is needed to extract the absolute temperature and have highest frame rates when using special digitalization process of around 30 kHz [3]. Micro-Raman thermography is another temperature measurement technique using the dependency of the temperature with the phonon frequency. It has a higher spatial resolution, it being of $\sim$0.5 μm, this spatial resolution depends on the wavelength and on the spot of the laser [4], however the acquisition time is long; depending on the material under study it can take from seconds to several minutes to obtain the temperature of a single point [5]. Another temperature measurement with high spatial resolution ($0.3 - 0.5$ μm) is the transient thermoreflectance imaging which uses an ultrashort laser pulse to excite the material and a weaker probe beam to detect the transient reflectance [2], [6]. However, the thermoreflectance coefficients depend on the wavelength, material and texture of the surface, so it is important to do an *in-situ* calibration [7]. Fluorescent microthermographic imaging technique has a spatial resolution of 0.3 μm, however, for using this technique a fluorescent layer has to be deposited on the sample under study [8], even when using fluorescence intensity ratio for getting low cost and fast response [9].

Two-colour fiber-optic pyrometry overcomes some of those issues. It is a non-contact technique, that allows an absolute

Manuscript received September 1, 2020; revised September 2, 2020; accepted September 3, 2020. Date of publication September 7, 2020; date of current version January 6, 2021. This work was supported in part by the Spanish Ministry of Science, Innovation and Universities Grant RTI2018-094669-B-C3 and Juan de la Cierva Grant FJCI-2017-31677, in part by the Directorate for Research and Innovation at Madrid region Grants P2018/NMT-4326, Y2018/EMT-4892 and INTECSOLARIS-CM-UC3M; and in part by FSE. The associate editor coordinating the review of this article and approving it for publication was Dr. Carlos Marques. *(Corresponding author: C. Vázquez.)*

The authors are with the Displays and Photonics Applications Group, Electronics Technology Department, Carlos III University of Madrid, 28911 Madrid, Spain (e-mail: arnunezc@ing.uc3m.es; atapetad@ing.uc3m.es; cvazquez@ing.uc3m.es).

Digital Object Identifier 10.1109/JSEN.2020.3022179

temperature measurement without knowing the emissivity of the material, because it can be used as a self-reference technique using two wavelength bands [10]–[12] as in other fiber-optic intensity sensors [13]. The selected bands should be close to provide the same material emissivity but far apart to allow filtering and reduce measurement errors [14]. The spatial resolution of this technique depends on the optical fiber that is used, and on the distance between the optical fiber and the measured object. Different optical fibers, made of different materials, with different core and cladding sizes, and different numerical apertures have been proposed in literature [10], [11], [14]–[21]. The amount of collecting light depends on those parameters. Most of those pyrometers use optical fibers with core diameters from 1 mm [10] to 280 μm [18], and using different photodetectors at both channels. Meanwhile in [14], [22], selecting closer channels bands allows using identical photodetectors at both channels that in conjunction with a low insertion loss demultiplexing technique makes feasible using optical fibers with core diameters of 62.5 μm. This pyrometer has a limited dynamic range of around 400°C.

An additional element, an optical switch that is powered by light, is used in [15] along with low-noise photodetectors and high-gain transimpedance amplifiers, to compensate for undesirable offsets in the receiving signal, but with the same limited dynamic range and spatial resolution of [14], [22]. With the data provided in those works we estimate the measuring area, related with the spatial resolution, of each pyrometer, it being in the range of 77 to 1010 μm at a distance of 25 μm. Higher spatial resolution requires using a smaller core diameter and numerical aperture, so for the same temperature the collecting light is lower. This allows a wider dynamic range by optimizing the overall optical losses, optoelectronics and conditioning circuits including new photodetectors, and demultiplexers. In this work, we propose a low cost, fast two-colour pyrometer that has the highest spatial resolution reported to date for a wide temperature range, by using a single mode standard optical fiber, narrow channel bands, no cooling photodetectors and a single high gain amplifier. This proposal is compared with previously reported optical fibers pyrometers and is shown the improvement on the current set-up for a specific temperature range. Theoretical analysis and measurements for different pyrometer configurations are reported.

II. Theoretical Background and State of the Art

Pyrometry is based on measuring the spectral radiance (L) of an object, and thus it is governed by the Planck's law; however, as the real bodies are not perfect emitters, the emissivity (ε) of the body has to be taken into account as shown in Eq. (1):

$$L(\lambda, T) = \frac{C_1 \cdot \varepsilon(\lambda, T)}{\lambda^5 \cdot \left(e^{C_2/\lambda T - 1}\right)} \tag{1}$$

where, C_1 ($1.191{\cdot}10^8$ $\mathrm{W{\cdot}Sr^{-1}} \cdot \mu\mathrm{m^4{\cdot}m^{-2}}$) and C_2 ($1.439{\cdot}10^4 \mu\mathrm{m{\cdot}K}$) are the Planck's radiation constants, λ is the wavelength and T is the absolute temperature of the body.

In particular, in a two-colour fiber optic pyrometer, the infrared rays emitted by the object are recovered by the optical fiber and then separated into different wavelength bands, finally the radiation is converted into an electrical signal using photodetectors. However, only the rays inside the acceptance cone of the optical fiber reach the photodetectors. This acceptance cone depends on:

- the numerical aperture (NA) of the fiber depending on the refractive index of the core (n_{core}) and the cladding ($n_{cladding}$) as follows:

$$\mathrm{NA}(\lambda) = \sqrt{\mathrm{n_{core}^2 - n_{cladding}^2}} \tag{2}$$

- optical fiber location with respect to the target surface.

Assuming that the optical fiber is placed perpendicular to the target surface which can be considered as an infinite surface, $\mathrm{R_T} \gg \mathrm{R_{NA}}$, see Fig. 1, the photocurrent generated in a photodetector ($\mathrm{I_D}$) for a specific spectral band is given by:

$$\mathrm{I_D(T,\lambda)} = \int_{\lambda_A}^{\lambda_B} \frac{\mathrm{C_1 \cdot R(\lambda) \cdot L(\lambda) \cdot \alpha(\lambda) \cdot \varepsilon(\lambda, T)}}{\lambda^5 \cdot \left(e^{C_2/\lambda T - 1}\right)} \cdot \frac{\pi^2 \cdot \mathrm{d_{core}^2}}{8} \cdot [1 - \cos(2 \cdot \theta_{\max}(\lambda))] \cdot \mathrm{d}\lambda \tag{3}$$

where $\theta_{\mathrm{Max}} = \arcsin(\mathrm{NA})$ is the acceptance angle limiting the acceptance cone, λ_A and λ_B are the shortest and longest wavelengths of specific wavelength band of the two-colour pyrometer, R is the photodetector responsivity, IL is the insertion loss at each wavelength band, α is the fiber attenuation coefficient, and d_{core} is the core diameter. Including the transimpedance amplifier of the detector, the output voltage ($\mathrm{V_D}$) is given by:

$$\mathrm{V_D(T,\lambda)} = \mathrm{I_D(T,\lambda)} \cdot G + \mathrm{V_{Noise}} \tag{4}$$

where G is the amplifier transimpedance gain and $\mathrm{V_{Noise}}$ is a factor which includes all the noise terms: Shot, Thermal and Dark noises, along with the offset voltage at the output of the detector.

In both cases, in a two-colour pyrometer, if the selected wavelength channels are closer enough, the emissivity of the surface can be discarded, so it is possible to use the ratio between them to obtain the temperature (T_R) of the material as follows:

$$T_R = \left(\frac{1}{T} + \frac{\ln(\varepsilon_R \cdot \delta_R)}{C_2 \cdot \left(\frac{-4 \cdot \Delta\lambda}{4 \cdot \lambda_C^2 - \Delta\lambda^2} \right)} \right)^{-1} \tag{5}$$

where λ_c is the average central wavelength ($\lambda_c = (\lambda_2 + \lambda_1)/2$), $\Delta\lambda$ is the wavelength spacing of the single wavelength channels ($\Delta\lambda = \lambda_2 - \lambda_1$), ε_R is the emissivity ratio ($\varepsilon_R = \varepsilon_{\lambda_1}/\varepsilon_{\lambda_2}$), δ_R is the loss ratio ($\delta_R = \mathrm{R_{\lambda_1} \cdot \alpha_{\lambda_1} \cdot L_{\lambda_1} \cdot \kappa_{\lambda_1} / R_{\lambda_2} \cdot \alpha_{\lambda_2} \cdot L_{\lambda_2} \cdot \kappa_{\lambda_2}}$), T is the calibrated temperature.

The selected bands are close to provide the same material emissivity but far apart to allow filtering and reduce measurement errors [14]. Even more, each selected band has a specific bandwidth not considered in Eq (5) but in Eq. (3) that determines the dynamic range, limited by the system saturation in the real pyrometer. So, the selected bands and the respective bandwidth, depending on the filter and photodetectors, have to be selected for each specific pyrometer.

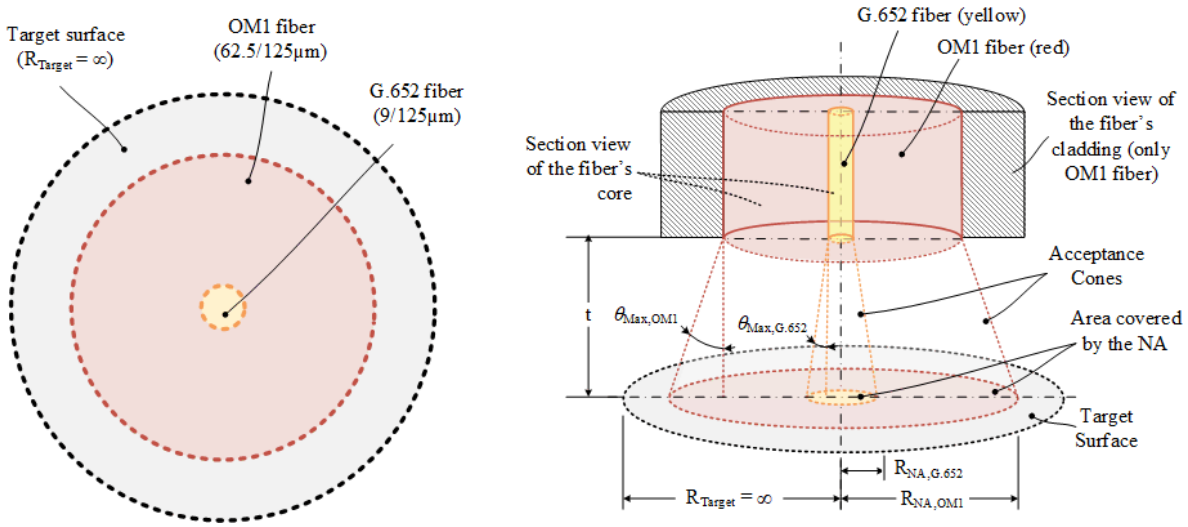

Fig. 1. Scaled drawing of the measuring area covered by the NA of the OM1 and G.652 glass optical fibers on a target surface.

TABLE I
COMPARISON BETWEEN DIFFERENT TWO-COLOUR OPTICAL FIBER PYROMETERS FOUND IN LITERATURE AND THIS WORK

Ref.	Fiber (diameter in mm)	NA (a.u.)	Spatial resolution (µm)	Temperature range (°C)
[20]	Unknown fiber material ϕ_{Fiber} = 1 mm	Unknown (collimation lenses)	10000[1]	55 to 245 C (Lock-amplifier and cooling)
[10]	Quartz optical fiber ϕ_{Core} = 1 mm	0.22	1011	200 to 1200 C
[16]	Fluoride glass optical fiber ϕ_{Core} = 450 µm ϕ_{Clad} = 500 µm	0.2	460	200 to 800 C
[19]	Crystalline Sapphire ϕ_{Fiber} = 425 µm	~ 0.19	434	200 to 1000 C
[18]	Doped glass optical fiber ϕ_{Clad} = 280 µm	0.21[2]	291	500 to 1000 C
[17]	Quartz optical fiber ϕ_{Core} = 50 µm ϕ_{Clad} = 75 µm	0.29	65	700 to 1100 C
[14], [15]	OM1 glass optical fiber ϕ_{Core} = 62.5 µm ϕ_{Clad} = 125 µm	0.275	77	200 to 575 C
[11]	Silica optical fiber ϕ_{Core} = 100 µm ϕ_{Clad} = 140 µm	0.22	111	900 to 1100 C
[21]	Chalcogenide glass fiber ϕ_{Core} = 400 µm	(chopper, collimation lenses)	Worse than 400	100 to 450 C
This Work	G.652 glass optical fiber ϕ_{Core} = 9 µm ϕ_{Clad} = 125 µm	0.14	16	300 to 1200 C

Notes: (1) The measuring area is calculated from Fig. 3 extrapolating the spot diameter from the distance between screw holes of the optical table. (2) Optional plug-in with lens-head is available.

The measured area (S_{NA}) of the pyrometer depends on its acceptance angle (θ_{Max}), and the distance (t) between the fiber and the target surface as follows:

$$S_{NA} = \left(t \cdot \tan\theta_{Max} + \frac{d_{core}}{2}\right)^2 \cdot \pi \quad (6)$$

To analyse the influence of the fiber properties on the spatial resolution, a comparative analysis is carried out in Table I. In all cases the spatial resolution is defined as the diameter of the light spot calculated from Eq. (6), taking a distance between the fiber end and the target surface of 25 μm. Table I demonstrates the widespread use of large core fiber diameters in pyrometry applications to enhance the light gathering [10], [16], [19]. Some proposals also include optical lenses placed at the fiber end to help the probe to improve the light gathering and focusing capabilities [20]. These improvements allow the designers to reduce the minimum measurable temperature, which is highly dependent on the photodetector noise and the system losses, among others [14]. On the contrary, the use of large diameters and dedicated lenses limits the use of these pyrometers in applications where high spatial resolutions and hard measuring conditions are required. As an example, for

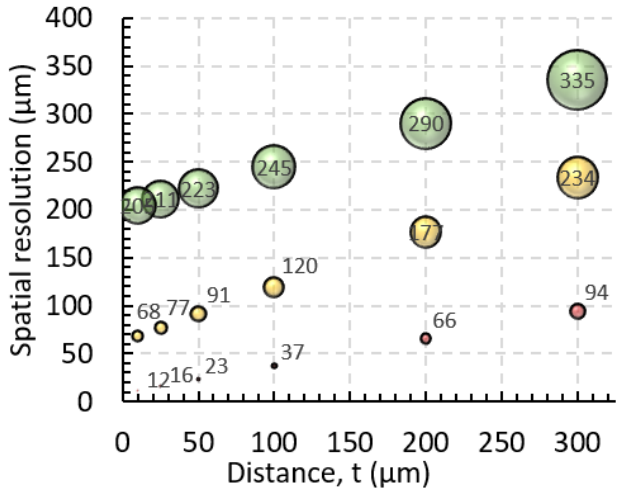

Fig. 2. Spatial resolution versus the optical fiber probe distance to the target surface for three fibers with different core diameter and numerical aperture: green 200 μm/0.2, yellow: 62.5 μm/0.275, red: 9 μm/0.14.

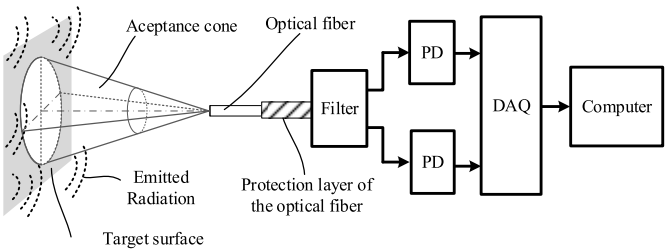

Fig. 3. Experimental two-colour optical fiber pyrometer set-up.

microthermography applications in machining processes, small fiber diameters as the one proposed in this work, allows to achieve spatial resolutions up to 16 μm at a distance of 25 μm, the highest reported to date, more than 5 times than previous works [17], [22] and for a wider temperature range.

In this sense, the proposed sensor also shows a low price as the one reported in [11] because of the inherent benefits of using commercial off-the-shelf optical fibers and opto-electronic devices well stablished on optical communication networks.

The spatial resolution versus optical fiber probe distance to the target surface is shown in Fig. 2 for different commercial fibers. It can be shown that the spatial resolution enhancement of using G.652 optical fiber can be up to 5 times in comparison with 200 μm diameter optical fibers with NA of 0.2 at a 200 μm distance to target surface. The effect of NA on spatial resolution degrades as the distance target increases, as expected.

III. Experimental Set-up

The two-colour optical fiber pyrometer set-up is shown in Fig. 3. It is formed by a standard optical fiber, in this experiment two types of those optical fibers are used:

- A multimode optical fiber (MMF) OM1 with core/cladding diameters of 62.5/125 μm and a NA of 0.275.
- A single mode optical fiber (SMF) G.652 with core/cladding diameters of 9/125 μm and a NA of 0.14.

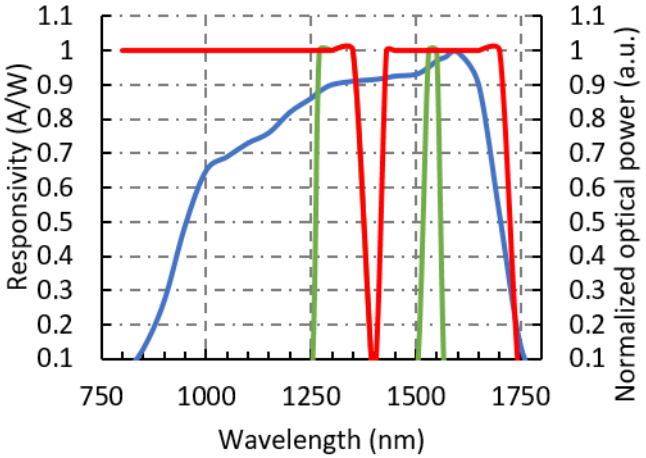

Fig. 4. (Left axis) InGaAs photodetector responsivity (blue) and (right axis) WDM SMF (green) and MMF (red) filters spectra response approximation for both bands centered at 1310 nm and 1550 nm.

The length of the fibers is of 0.5 m. Then, a low insertion loss WDM optical filter splits the radiation into two spectral bands; they are centred at 1.31 μm and 1.55 μm respectively. The bandwidth of each filter wavelength bands is different for each type of fiber as shown in Fig. 4. The two InGaAs photodetectors (PD), working in the 800-1700 nm spectral range, include transimpedance amplifiers. They can be set in high gain (HG) or low gain (LG) with a bandwidth of 0.5 kHz for HG and 2 kHz for LG. They convert the optical radiation into an electrical signal that is recorded by a data acquisition card (DAQ) connected to a PC. The absolute accuracy of the DAQ at full scale is of 2688 μV for the 10 V range.

For the measurements, a dry block calibrator (Jupiter 650, *Isotech*) equipped with a black body is used. This equipment has a control unit that ensures the temperature stability at $\pm$0.03°C and the uncertainty at $\pm$0.17 °C in the range of 50 to 650 °C. The calibration is done from 150 to 650 °C with steps of 25 °C. For maximizing the stability of each temperature, an interval of time of 45 min was considered. On the other hand, the black body has an emissivity of 0.99.

The optical fibers are situated at 0.3 mm from the black body surface, this is done with a calibrated metallic holder that ensures the position of the fibers. With all these data and with Eq. (6), it is possible to extract the surface that is going to be measured with each fiber (S_{NA}), see Fig. 2.

The DAQ card is configured to measure both wavelength channels with a sampling rate of 1 kHz and taking 500 samples per temperature. The average output voltage and standard deviation from each temperature and at each wavelength channel are calculated from the recorded samples.

IV. Results and Discussion

The experiments were carried out using the black body on a dry block calibrator as explained in the previous section. Two different pyrometers are developed, either equipped with SMF or MMF fiber and different filters as a function of the spatial resolution that is needed in each application. As shown in Fig. 4 the filter splits the recovered energy by the fiber into

two different bands one centred at 1310 nm and the other at 1550 nm, with different spectral bandwidths around each channel.

The theoretical calculations describing the pyrometer response are carried out taking into account different approximations and assumptions to adapt the mathematical expressions to the characteristics of the different elements of the pyrometer. All of them are described as follows:

- The NA of the optical fiber is calculated from the relation between the refractive index of the core and cladding of Eq. 2. Those refractive indexes depend on wavelength and can be fit to a three-term Sellmeier dispersion relation:

$$n(\lambda) = \left[1 + \sum_{i=1}^{3} \frac{A_i \cdot \lambda^2}{\lambda^2 - l_i^2}\right]^{1/2} \quad (7)$$

where n is the refractive index either of the core or of the cladding, A_i is the oscillator strength and l_i is the oscillator wavelength [23].

The mathematical expression of the NA as a function of the wavelength is introduced in Eq. (3) through the acceptance cone to perform symbolic computations.

- The insertion loss of the optical filter is calculated as the insertion loss at the mean value of the selected channel band. A flat response is assumed because changes of the insertion losses along the channel band are negligible and have no significant influence on the intensity of the light.
- The attenuation of the fiber is selected following the same procedure as the insertion loss of the optical filter. The mean value of the selected channel band is chosen to fix its value. There is no significant change on the light intensity when other close attenuations are computed.
- The conversion factor is a parameter which encompasses the photodetector responsivity and the transimpedance amplifier gain. This value depends on the conditioning circuit. and in this work is obtained by experimental methods, launching optical power into the sensing area and measuring the output voltage with a voltmeter. This value changes for the different channel bands used in the experimental setup.
- The detector voltage noise is also obtained by experimental methods.

A summary of the parameters taking into account in the theoretical analysis for all opto-electronics components is reported in Table II:

A numerical value of the voltage is calculated for different temperatures, considering all the previous assumptions and approximations in the mathematical expression of the output voltage of Eq. (4). All calculations are performed with the Symbolic Math Toolbox of MATLAB.

In terms of measurements, first, the pyrometer was equipped with a multimode optical fiber and filter to collect the radiation of the heated body. Fig. 5 shows the measured voltage when increasing the black body temperature from 150 to 650°C in steps of 25°C and the theoretical results from Eqs. (3-4) and adapted losses, when the PD are set in both high and low gain, HG and LG respectively.

TABLE II
SUMMARY OF THE OPTO-ELECTRONICS PARAMETERS OF THE DEVICES USED DURING THE THEORETICAL ANALYSIS

Parameter	Value
Insertion losses of the optical filber (IL) at 1310 nm, dB	0.21
Insertion losses of the optical filber (IL) at 1550 nm, dB	0.06
Fiber attenuation (α) at 1310 nm, dB	0.58
Fiber attenuation (α) at 1550 nm, dB	0.28
Conversion factor at 1310 nm, V/W	$9{\cdot}10^8$
Conversion factor at 1550 nm, V/W	$8{\cdot}10^8$
Voltage noise, mV	13.6

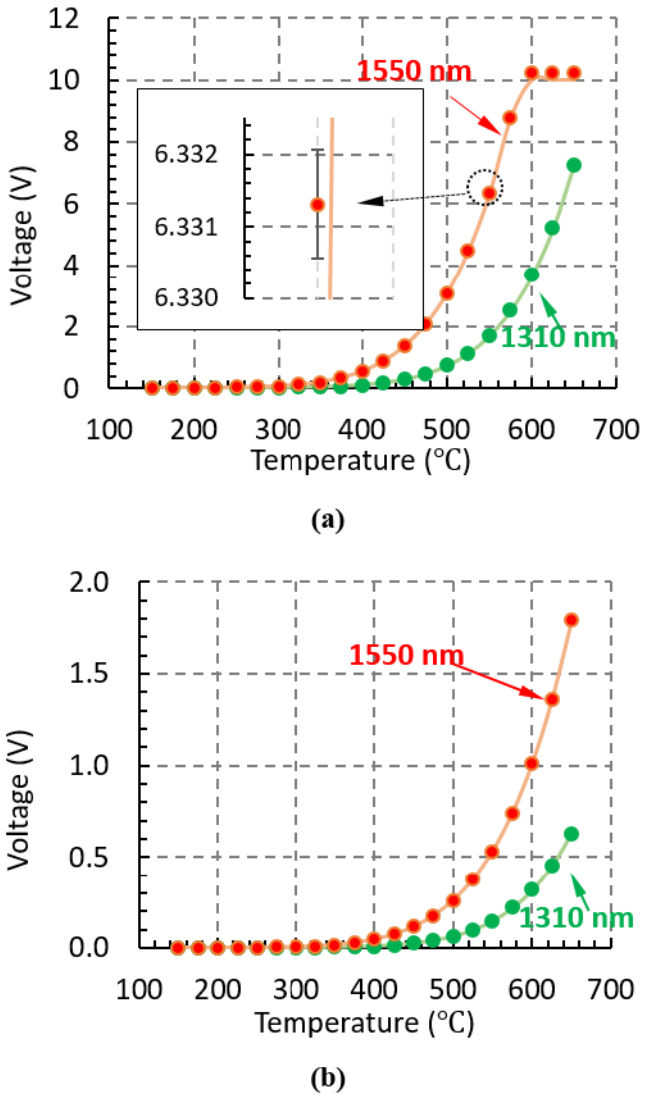

Fig. 5. Measurements (dots) using the black body in the dry block calibrator and simulations (lines) obtained for the two-colour pyrometer with MMF and the photodetectors set at: a) high gain, a zoom of one measurement has been done in order to show the measurement standard deviation and b) low gain.

For HG (Fig. 5a), the voltage collected in the channel centred at 1550 nm is saturated for temperatures above 600°C, the saturation of the signal comes from the maximum voltage

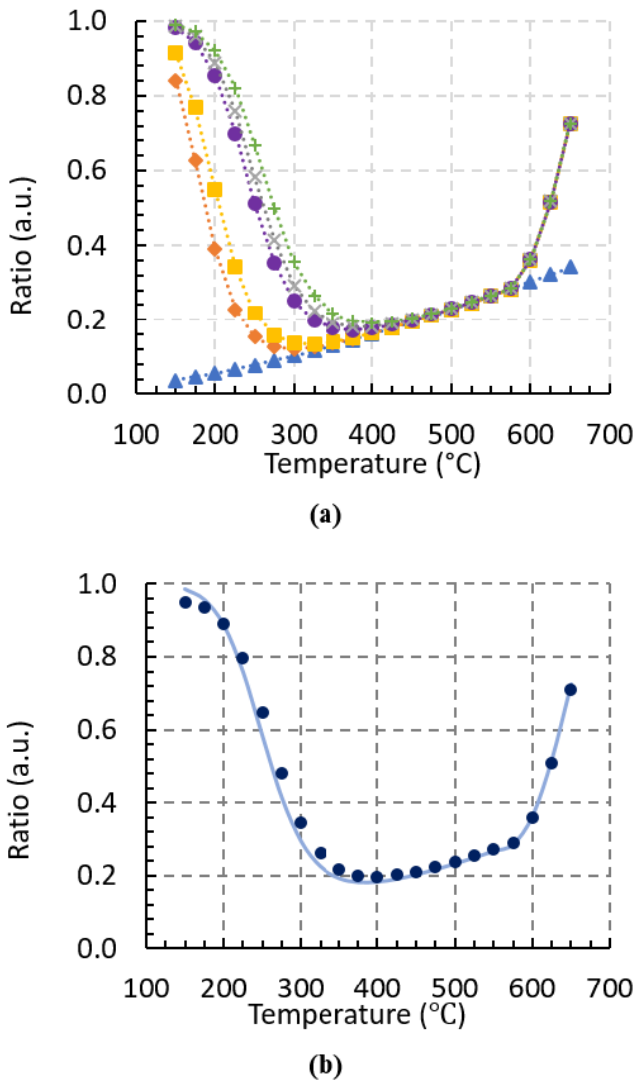

Fig. 6. a) HG MMF pyrometer ratio theoretical analysis with DAQ saturation, PD offset and noise: 0 mV (triangles) and no DAQ saturation (ideal), 1 mV (diamonds), 2 mV (squares), 10 mV (dots), 14 mV (×), 20 mV (+). b) Experimental (dots) and theoretical (lines) ratio for HG MMF pyrometer.

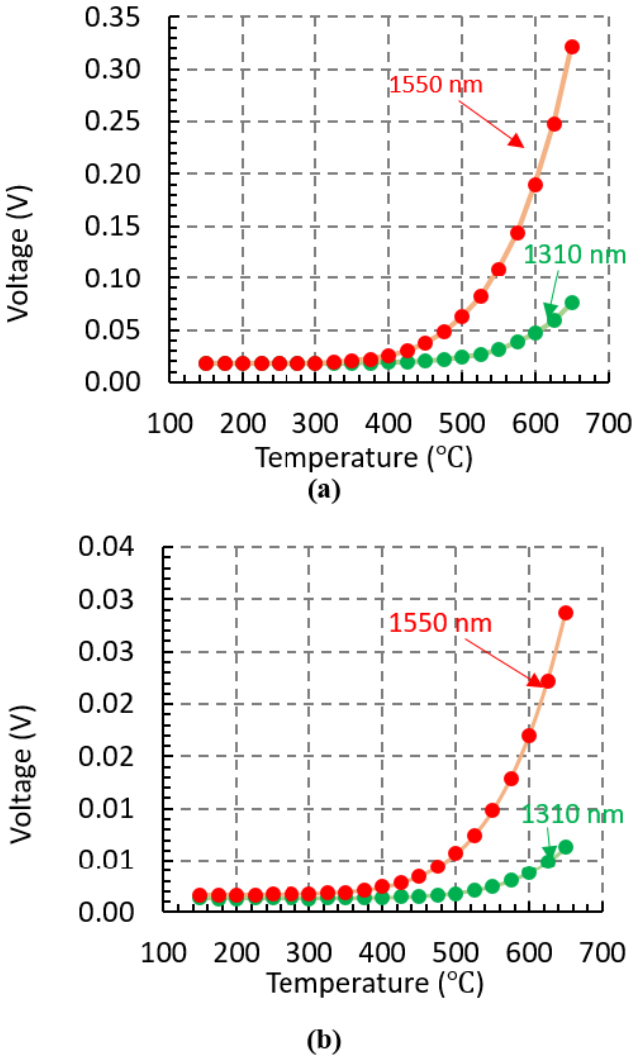

Fig. 7. Experimental (dots) using the black body in the dry block calibrator and theoretical analysis (lines) results obtained for the two-colour pyrometer with SMF and the photodetectors set at: a) high gain and b) low gain.

that can read the DAQ card which is limited to 10 V. This implies that the pyrometer with the MMF and the PD set in HG has an operation range from 200 to 575°C. On the other hand, when using the photodetectors in LG, see Fig. 5b, the operation range in this configuration is larger. The zoom in Fig. 5a shows the standard deviation of the measurements, it being in the worst case of ±2.1 mV for 1310 nm and ±1 mV for 1550 nm at HG and of ±0.6 mV for both wavelengths at LG.

The two-colour pyrometer can use the voltage ratio (this is, 1310/1550) of the measuring channels in order to avoid the emissivity influence. We show in Fig. 6 the ratio for both configurations. The theoretical results fit quite well the experimental ones (see Fig. 6b). Typical two-colour pyrometers [10], [14] show a linear relationship between the output ratio and the temperature with a positive slope. In our case, we have an almost planar zone for temperatures below 200°C, this zone is extremely affected by the noise and offset of the photodetectors that are overall of 1.38 mV (LG) and 13.6 mV (HG). The straight line with triangles on Fig. 6a represents the pyrometer ratio without PD noise and offset, neither saturation from DAQ card. Different noise and offset values from 1 to 20mV are considered, their influence is clear from 200 to 375°C. And the consequence is the negative slope of the ratio versus the temperature, because the energy recovered by the channel centred at 1310 nm is low, although higher than the noise of the photodetectors but the one centred at 1550 nm is higher. The positive slope means that the energy centred at 1550 nm starts to increase faster. The last change in the slope shown in Fig. 6, is due to the DAQ card saturation of the channel centred at 1550 nm, as previously shown in Fig. 5a.

The same experiment was done equipping the pyrometer with a single mode optical fiber and filter, and the results are shown in Fig. 7.

When using SMF fiber, the voltage is far away from the saturation, it is important to have in mind that with the DAQ

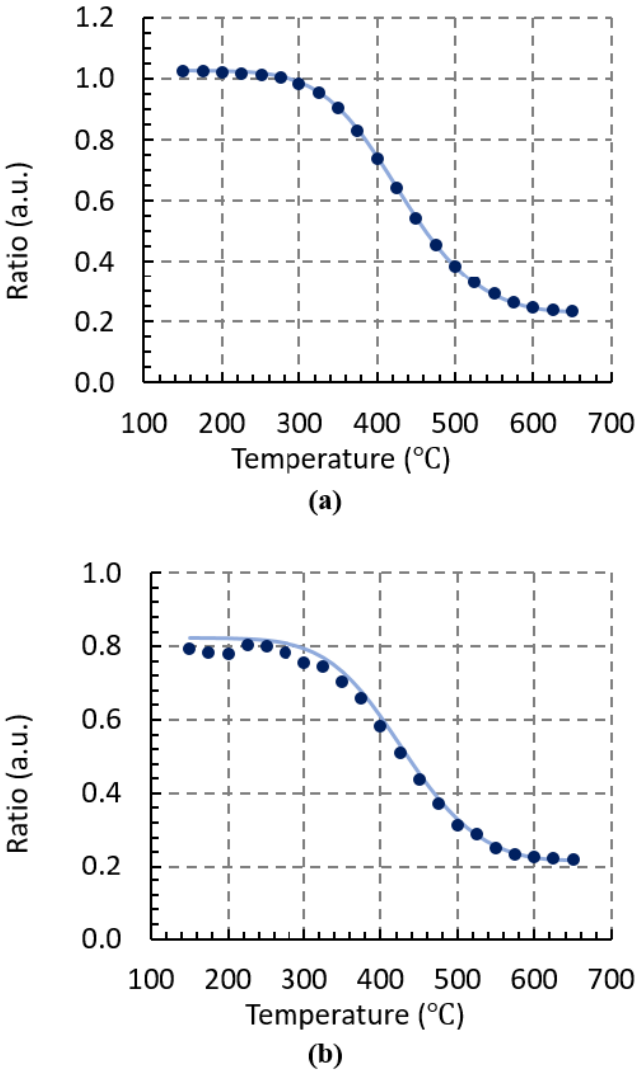

Fig. 8. Experimental (dots) and theoretical (lines) ratio for the SMF two-colour pyrometer with the photodetectors set at: a) high and b) low gain.

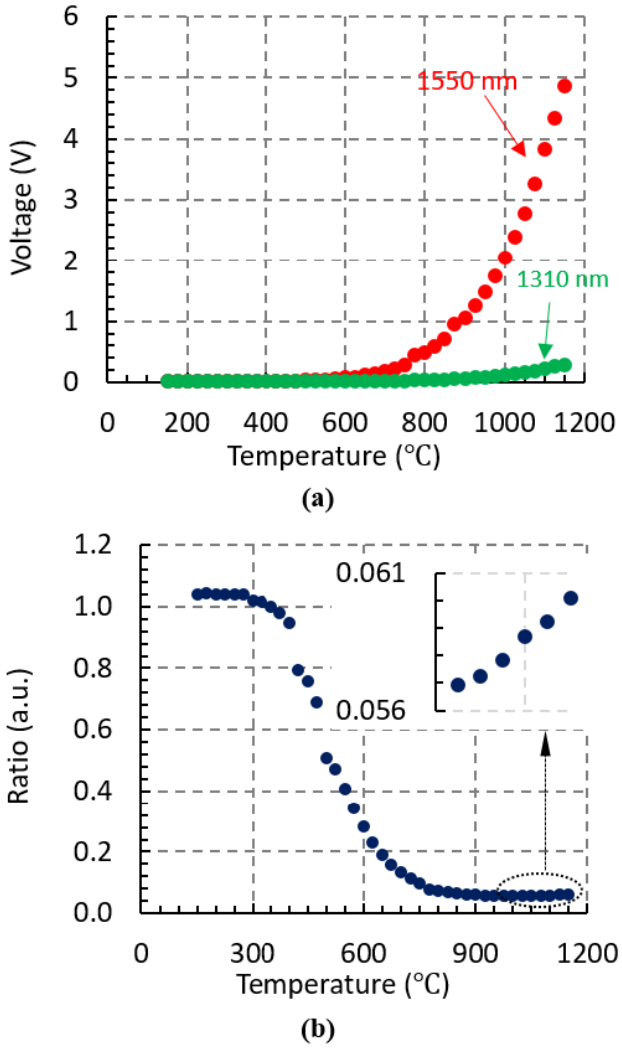

Fig. 9. Experimental results of the two-colour SMF optical fiber pyrometer set at HG: a) voltage-temperature relationship for both channels, b) ratio-temperature relationship.

card we are using, the voltage range is limited to 10 V. SMF fiber allows measuring higher temperatures than with MMF. The lower diameter and numerical aperture of the optical fiber, and the narrow channels bandwidths of the filter limit the energy recovered. However, the minimum temperature now decreases, as shown in Fig. 8. The noise and offset of the photodetectors in this case affect the measurements in terms of avoiding any temperature related variations up to 300°C for both low and high gain. In this case, the positive slope of the pyrometer is not shown due to the temperature range considered.

In order to better explore the temperature measurement range of the two-colour SMF optical fiber pyrometer, a new dry block calibrator (Pegasus 1200, *Isotech*) has been used. This dry block calibrator works from 150 to 1200°C with a stability of ±0.05 to ±0.2°C, respectively.

Fig. 9 shows the experimental results of (a) the voltage of both channels and (b) the ratio of those voltages of the two-colour pyrometer when using the SMF fiber and setting the photodetectors in HG. As explained before, the noise and offset of the photodetectors affect the measurements up to 300°C, then the negative slope of the ratio is seen. Finally, the linear part is shown for temperatures above 600°C, see the inset on Fig. 9b.

This pyrometer can be used in machining Inconel 718 requiring fast response, as we have previously reported with a MMF pyrometer [24] in experiments with cutting speeds up to 180 m/min and a feed rate of 0.1 mm/rev. Using this new pyrometer will improve the spatial resolution and temperature span. On the other hand, the possibility to measure at low temperatures using other types of fibers such as polymer optical fibers should also require a mechanical analysis [25]–[27].

V. Conclusion

In this work, we have reported a two-colour optical fiber pyrometer with high spatial resolution, wide dynamic range and fast response. The system uses standard single mode

optical fibers and related devices providing a low cost along with low-noise photodetectors and single high-gain transimpedance amplifiers. The developed pyrometer presents the highest spatial resolution reported in this technology, it being of 16 μm for a target surface at 25 μm in a temperature range of 300 to 1200°C, with a sampling rate of 1 kHz. This high spatial resolution allows its use in applications requiring fast measurements in small spots in difficult to access areas where the temperatures are high, as in microthermography applications in machining processes. Experimental and theoretical results have been done in order to show the potential of the two-colour optical fiber pyrometer.

ACKNOWLEDGMENT

The authors thanks L. G. Jiménez for her work in the theoretical analysis of the two color optical fiber pyrometer.

REFERENCES

[1] K. P. Möllmann and M. Vollmer, "IR imaging of microsystems: Special requirements, experiments and applications," in *Proc. Int. Conf. Infr. Sensors Syst.*, 2011, pp. 5–10.
[2] S. Jorez, J. Laconte, A. Cornet, and J.-P. Raskin, "Low-cost optical instrumentation for thermal characterization of MEMS," *Meas. Sci. Technol.*, vol. 16, no. 9, pp. 1833–1840, Sep. 2005.
[3] R. Usamentiaga, P. Venegas, J. Guerediaga, L. Vega, J. Molleda, and F. Bulnes, "Infrared thermography for temperature measurement and non-destructive testing," *Sensors*, vol. 14, no. 7, pp. 12305–12348, Jul. 2014.
[4] P. Löw, B. Kim, N. Takama, and C. Bergaud, "High-spatial-resolution surface-temperature mapping using fluorescent thermometry," *Small*, vol. 4, no. 7, pp. 908–914, Jul. 2008.
[5] B. Öner, J. W. Pomeroy, and M. Kuball, "Submicrometer resolution hyperspectral quantum rod thermal imaging of microelectronic devices," *ACS Appl. Electron. Mater.*, vol. 2, no. 1, pp. 93–102, Jan. 2020.
[6] R. J. Stevens, A. N. Smith, and P. M. Norris, "Signal analysis and characterization of experimental setup for the transient thermoreflectance technique," *Rev. Sci. Instrum.*, vol. 77, no. 8, pp. 1–8, 2006.
[7] K. Yazawa and A. Shakouri, "Ultrafast submicron thermoreflectance imaging," *Electron. Cool. Mag. Spring*, vol. 10, pp. 10–12, Mar. 2011.
[8] D. L. Barton, "Fluorescent microthermographic imaging," in *Proc. 20th Int. Symp. Test. Failure Anal.*, 1994, pp. 87–95, doi: 10.1017/CBO9781107415324.004.
[9] J. Xiong *et al.*, "Real-time micro-scale temperature imaging at low cost based on fluorescent intensity ratio," *Sci. Rep.*, vol. 7, no. 1, p. 41311, Feb. 2017.
[10] B. Müller and U. Renz, "Development of a fast fiber-optic two-color pyrometer for the temperature measurement of surfaces with varying emissivities," *Rev. Sci. Instrum.*, vol. 72, no. 8, pp. 3366–3374, Aug. 2001.
[11] F. J. Madruga, D. A. F. Fernandez, and J. M. Lopez-Higuera, "Error estimation in a fiber-optic dual waveband ratio pyrometer," *IEEE Sensors J.*, vol. 4, no. 3, pp. 288–293, Jun. 2004.
[12] C. Vázquez, A. Tapetado, H. Miguélez, and J. Díaz-Álvarez, "Two-colour fibre optic pyrometer," U.S. Patent WO 2016170213 A1, Oct. 27, 2016.
[13] D. S. Montero and C. Vázquez, "Remote interrogation of WDM fiber-optic intensity sensors deploying delay lines in the virtual domain," *Sensors*, vol. 13, no. 5, pp. 5870–5880, May 2013.
[14] A. Tapetado, J. Díaz-Alvarez, M. H. Miguélez, and C. Vázquez, "Two-color pyrometer for process temperature measurement during machining," *J. Lightw. Technol.*, vol. 34, no. 4, pp. 1380–1386, Feb. 15, 2016.
[15] C. Vázquez *et al.*, "Fiber-optic pyrometer with optically powered switch for temperature measurements," *Sensors*, vol. 18, no. 2, pp. 1–10, 2018.
[16] J. Thevenet, M. Siroux, and B. Desmet, "Measurements of brake disc surface temperature and emissivity by two-color pyrometry," *Appl. Thermal Eng.*, vol. 30, nos. 6–7, pp. 753–759, May 2010.
[17] T. Ueda, M. Sato, T. Sugita, and K. Nakayama, "Thermal behaviour of cutting grain in grinding," *CIRP Ann.*, vol. 44, no. 1, pp. 325–328, 1995.
[18] D. Hernandez, G. Olalde, A. Beck, and E. Milcent, "Bicolor pyroreflectometer using an optical fiber probe," *Rev. Sci. Instrum.*, vol. 66, no. 12, pp. 5548–5551, Dec. 1995.
[19] A. Heeley, M. Hobbs, H. Laalej, and J. Willmott, "Miniature uncooled and unchopped fiber optic infrared thermometer for application to cutting tool temperature measurement," *Sensors*, vol. 18, no. 10, p. 3188, Sep. 2018.
[20] M. Willsch, T. Bosselmann, D. Gaenshirt, J. Kaiser, M. Villnow, and M. Banda, "Low temperature fiber optic pyrometer for fast time resolved temperature measurements," *Proc. SPIE*, vol. 9916, May 2016, Art. no. 99160R.
[21] T. Koyano, T. Takahashi, S. Tsurutani, A. Hosokawa, T. Furumoto, and Y. Hashimoto, "Temperature measurement of wire electrode in wire EDM by two-color pyrometer," *Procedia CIRP*, vol. 68, no. 4, pp. 96–99, 2018.
[22] A. Tapetado, J. Díaz-Alvarez, H. Miguélez, and C. Vázquez, "Fiber-optic pyrometer for very localized temperature measurements in a turning process," *IEEE J. Sel. Top. Quantum Electron.*, vol. 23, no. 2, pp. 1–6, Mar. 2017.
[23] I. H. Malitson, "Interspecimen comparison of the refractive index of fused silica," *J. Opt. Soc. Amer.*, vol. 55, no. 10, p. 1205, 1965.
[24] J. Díaz-Álvarez, A. Tapetado, C. Vázquez, and H. Miguélez, "Temperature measurement and numerical prediction in machining Inconel 718," *Sensors*, vol. 17, no. 7, p. 1531, 2017.
[25] A. G. Leal-Junior, C. Marques, A. Frizera, and M. J. Pontes, "Dynamic mechanical analysis on a polymethyl methacrylate (PMMA) polymer optical fiber," *IEEE Sensors J.*, vol. 18, no. 6, pp. 2353–2361, Mar. 2018.
[26] A. Leal-Junior *et al.*, "Dynamic mechanical characterization with respect to temperature, humidity, frequency and strain in mPOFs made of different materials," *Opt. Mater. Express*, vol. 8, no. 4, pp. 804–815, 2018.
[27] J. L. Pérez-Castellanos, D. S. Montero, C. Vázquez, J. Zahr-Viñuela, and M. González, "Photo-thermo-mechanical behaviour under quasi-static tensile conditions of a PMMA-core optical fibre," *Strain*, vol. 52, no. 1, pp. 3–13, 2016.

A. Núñez Cascajero received the M.E. degree in materials from Rey Juan Carlos University, Madrid, Spain, in 2011, and the Ph.D. degree from the Electronics Department, University of Alcalá, in 2017. In 2014, she was a Visiting Researcher with the CEA-Grenoble research Centre, France. During her Ph.D. she worked in III-V semiconductor materials, on its growth, characterization, and used as optical sensors, photoconductors, and solar cells. In 2018, she joined the Carlos III University of Madrid, Madrid, first in the Mechanical Engineering Department and then in the Displays and Photonic Application Group of the Department of Electronics Technology, where she is currently a Postdoctoral Researcher with a Juan de la Cierva grant. Her research main interests are materials, surface plasmon resonance sensors, solar cells, and optical fiber sensors.

A. Tapetado received the M.Sc. degree in industrial electronics engineering from the University of Castilla-La Mancha, Spain, in 2009, and the Ph.D. degree in electrical engineering, electronics, and automation engineering from the Carlos III University of Madrid, Spain, in 2015. He was a Visiting Student with the Aston Institute of Photonics Technologies, Aston University, U.K., in 2012, and with the Research Laboratory of Electronics, Massachusetts Institute of Technology, Cambridge, USA, in 2013, working on polymer optical fiber Bragg gratings, and silicon photonics, respectively. He is currently an External Researcher with the Display and Photonics Applications Group, Carlos III University of Madrid. In addition, he is working as a Instrumentation and Telemetry Engineer with the Smart Maintenance Engineering and New Project Department, Patentes Talgo, S.L.U. His research interests include polymer and silica fiber optics sensors, sensor networks, and its industrial applications.

C. Vázquez (Senior Member, IEEE) received the M.Sc. degree in physics (electronics) from the Complutense University of Madrid, Madrid, Spain, in 1991, and the Ph.D. degree in photonics from the Telecommunications Engineering School, Polytechnic University of Madrid, Madrid, in 1995. She received a fellowship at TELECOM, Denmark, in 1991, working on erbium-doped fiber amplifiers. From 1992 to October 1995, she worked at the Optoelectronics Division, Telefónica Investigación y Desarrollo. She was involved in III–V integrated optics devices characterization, design, and fabrication. In October 1995, she joined the Carlos III University of Madrid, Madrid, where she is currently a Full Professor with the Department of Electronics Technology and the Head of the Displays and Photonic Applications Group. She was a Visiting Scientist with the Research Laboratory of Electronics, Massachusetts Institute of Technology, from August 2012 to July 2013, working on silicon photonics. She was also the Head of the Department for three years and the Vice-Chancellor for four years. Her research interests include integrated optics, optical communications and instrumentation including, plastic optical fibers, broadband access networks and monitoring techniques, RoF systems, filters, switches, fiber optic sensors, and WDM networks. She has published more than 200 scientific publications and is the holder of five patents. She has participated in different European projects and networks in the ESPRIT, RACE, and IST framework programs such as PLANET, OMAN, HEMIND, SAMPA, EPhoton/One+, BONE (Building the Future Optical Network in Europe), and BlueSpace, and has led several national researching projects and consortium such as SINFOTON-CM. She is a Fellow of the SPIE.